Boffin Access

Open Access Journal | Volume: 2.2

Journal of Cancer Research and Oncobiology

ISSN 2517-7370

New Phenomenon in Living Matter?: Clusterization and Synchronization of Electrodynamic Landscape

Yuri Babich
Maya Nuzhdina

Center of the Skin Electrodynamic Introscopy, Kiev, Ukraine

Abstract

Our study aimed to reveal functional landscape/ heterogeneity of malignant and benign tumors at background of visibly healthy tissue as it seen in electrical bioimpedance parameters. The earlier developed method of the Skin Electrodynamic Introscopy (SEI), which had ever firstly already enabled adequate imaging the Skin Electrodynamic Landscape (SEL), proved also to be very sensitive in assessing the 2D skin dynamics in response to weak external stimuli. SEI uses a spectral electrical impedance method of measurement (modulus and phase of the impedance in the bandwidth of 2kHz-1MHz) which provides information on events happening at cellular and subcellular levels at 32 × 64 mm2 area with spatial resolution 1 mm. Nonthermal microwaves, weak magnetic field of therapeutic intensity, and hypoxia were used as test influences. Analysis of the multiparameter SEL of 7 cases of melanoma, 28 nevi and >50 cases of healthy skin revealed novel phenomena. In all melanomas, immergence of test-induced clusters of coherent activity, in-phase and out-of-phase synchronization of the SEL oscillations, accompanied by effects of inter-cluster interactions and propagations with a velocity up to 1 cm/min has been registered. The impact of magnetic field, in particular, was accompanied by the transitory effects of the global synchronizations. Their localization and intensity corresponded to visible tumor signs and, significantly exceeding them in details and prevalence, thus created thus a diverse landscape of hypo/hypersensitive structures. Such phenomena, but not so very pronounced and not so clearly associated with the lvisible nevi, were observed only in 2-3 cases, and never in health. These effects are presumably associated with cooperative mechanisms of short- and long-range of intercellular interactions. It seems quite predictable that these effects can emerge not only in the skin, but also in any tissues. The discovered phenomena may be helpful specifically for real-time mapping the tumor geometry and its affected surroundings, thus providing biofeedback and additional opportunities for cancer research, diagnosis, personalized treatment and surgery, as well as in various biomedical applications.

Keywords

Tumor; Clusters; Synchronization; Electrical impedance; Malignanization; Melanoma; Hypoxia; Intercellular interactions; Imaging; Diagnostics; Magnetic field; Microwaves

Abbreviations

MM: Malignant Melanoma

2D: Two Dimensional

SEL: Skin Electrical Impedance Landscape

SEI: Skin Electrodynamics Introscopy

MF: Magnetic Field

MF↓: Unipolar MF

MF↑↓: Reversing MF

MV: Mean Value

MW: Nonthermal MicroWaves

$|Z_k|$, $|Z_M|$: Electrical impedance modules at 2kHz and 1MHz (in k Ohms), respectfully

θ_k, $\theta_{M:}$ Phase angles at 2 kHz and 1 MHz (in degrees), (i.e. $Z=|Z|e^{i\theta}$)

ZMT: Zone of Maximum Transformations

AV: Averaged

σ-: Standard *deviation*

P: significance level

Introduction

Most studies of tumor heterogeneity have focused on genetic heterogeneity rather than on phenotypic heterogeneity that arises due to environmental selection forces

Article Information

DOI: 10.31021/jcro.20192123
Type: Research Article
Journal Type: Open Access
Volume: 2 **Issue: 2**
Manuscript ID: JCRO-2-123
Publisher: Boffin Access Limited

Received Date: 16 May 2019
Accepted Date: 19 July 2019
Published Date: 22 July 2019

***Corresponding author:**

Yuri Babich
Centre of the Skin Electrodynamic Introscopy
Kiev, Ukraine
E-mail: babich@ua.fm

Citation: Babich Y, Nuzdhina M. New Phenomenon in Living Matter: Clusterization & Synchronization of Electrodynamic Landscape. J Cancer Res Oncobiol. 2019 May;2(2):123

Copyright: © 2019 Babich Y. This is an open-access article distributed under the terms of the Creative Commons Attribution 4.0 international License, which permits unrestricted use, distribution, and reproduction in any medium, provided the original author and source are credited.

in the tumor. However, despite our growing knowledge about cellular heterogeneity in cancer, we are far from understanding the dynamics that operate among the heterogeneous subpopulations and their role in disease progression and therapeutic responses [1]. Cancer can be described by a *small number of functional ingredients*, despite the complexity of the pathology [2], but yet, the cooperative behavior of cancer cells and clones, that lead to the development of tumors, mostly remains as a theory with only a few experimental demonstrations and no mechanistic dissection of such cooperative interactions [3,4]. Several such studies conducted over the past few years have provided important insights into mechanisms that maintain heterogeneity and clonal cooperation within the tumors and how these can affect tumor behavior [1,4,5].

Recent perspectives propose that the breakdown of intercellular cooperation could depend on 'fields' and other higher-level phenomena, and could be even mutations independent. Indeed, the field would be the context, allowing (or preventing) genetic mutations to undergo an intra-organism process analogous to natural selection. The complexities surrounding somatic evolution call for integration between multiple incomplete frameworks for interpreting intercellular cooperation and its pathologies [6].

It is widely accepted that skin is a very complex, heterogeneous system which comprises different epidermal and dermal cell populations. In healthy skin these processes are tightly balanced, so the competition does not change the homeostatic limits. However, even in a healthy skin, recently, clones of cancer-driving mutations have been discovered. Around 140 mutations per square centimeter were found in the six focus genes [7]. Subsequently, it was demonstrated that mutant cells can have a competitive advantage over neighboring cells [8-10]. In a case of further tumorigenesis, the corresponding modification of processes of competition and collaboration leads to gradual loss of tissue architecture and distortion of its functional portrait. It would be therefore important to reveal and monitor these topological features.

Bioelectricity is a basic phenomenon associated with cellular and subcellular structures [11]. Most of the subcellular biomolecules (e.g. DNA, RNA, tubulin, actin, septin etc.) are either charged and hence surrounded by counter-ions or endowed with high electric dipole moments that can engage in dipole-dipole interactions and polarize electrically their local environment. Living organisms are replete with both moving and oscillating electric charges and can thus be regarded as complex electrochemical and mechanical systems [12].

Since cells and all types of tissues communicate electrically, it seems logical that the methods of studying these processes should be appropriate, i.e., in particular, providing dynamic visualization of the Skin Electrodynamic Landscape (SEL). Thus, research into electrical manifestation of spatio-temporal features of tumor and its micro- and macro-environment appears to us as a vital technical and biophysical and medical challenge.

In recent decades, the method of Electrical Impedance Spectroscopy (EIS) has been intensively developed, particularly in the field of diagnosing skin cancer [13-24]. It provides valuable information *in vivo* on the intercellular and intracellular environment, as well as on the integrity of cell membranes. The electrical impedance analysis of *single* cells can provide information on cells' pathological condition in various environments [25]. However, existing approaches on reading out the SEL do not provide a sufficiently high spatial resolution in large enough areas of the skin to obtain a coherent /unfragmented electrical portrait. However, even with these limitations, it becomes possible to detect small tumors and some tumor-related changes [26].

Our pioneering developments in the visualization and research into the phenomenology of the Skin Electrodynamic Landscape (SEL) began in the mid-1980s, when, with the aid of our early original experimental setup, firstly in the world, adequate static and, shortly, dynamic spectral images of the skin electrical landscape have been obtained. Studying the influence of various physicochemical factors (mechanical, nonthermal microwaves, magnetic fields, pharmaceuticals, and hypoxia) onto modification of the initial SEL in healthy and sick volunteers, we soon discovered a number of fundamental new spatio-temporal phenomena [27-33].

Summarizing, it can be said that SEL in healthy individuals has predominantly chaotic low-amplitude dynamics, for modification of which strong enough (up to painful/invasive) external stimuli are required. On the contrary, in a case of sickness/allergy of the same subject, the initial SEL becomes deeper and more structured; and even vanishingly weak stimuli can trigger a process of still more high-amplitude synchronous structuring in the form of pulsating or wavelike structures with characteristic velocity about the range of calcium waves of intercellular signaling. Such distinctly expressed functional heterogeneity of the SEL was observed in all cases of malignant melanoma (MM) (7 cases), and only in 3 (in a poorly expressed form) of 28 cases of benign neoplasms (nevi), and, under the same experimental conditions, never in healthy subjects (>50). This paper firstly presents a more detailed analysis of the discovered phenomena (both initial and test-induced ones) of functional clusterization of the MM area. Nonthermal microwaves (MW), magnetic field (MF), and hypoxia were used as testing stimuli. Two methodological approaches are examined: steady state measurements and complex spatial and/or temporal measurements.

Methods

Here we give only brief information about the method, which was described in more detail in [30]. In this study, we used the hypoxic test similarly to [30], but now the focus has been on the effects caused by MW and MF.

Hardware and measurement

The SEI experimental set-up is a portable autonomic device with a ±12 V battery power supply consisting of: sensor-head, measurement unit integrated in one box, a lab-top (Figure 1).

The sensory head of the SEI setup is a matrix of stainless steel 32 × 64 electrodes (304, Sandmeyer Steel Co., USA), 0.6 × 0.6 mm^2 each, making thus spatial resolution 1 mm (Figure 1). The measurement circuit includes: an active/running electrode, multiplexer, sinusoidal current generator (3 and 10 μA of 2 kHz and 1 MHz, respectfully), and a large (~10 cm^2) ground electrode (Figure 2). The large electrode is equivalent to an imaginary one being located interstitially in the most conductive deep layer of skin, i.e. dermis (connective tissue and intercellular liquid), enabling thus namely cross-sectional mode of measurement. Here we analyze only 4 out of 6 simultaneously measured parameters of impedance $Z=|Z|e^{i\theta}$: modules ($|Z_k|$, $|Z_M|$), and phase angles (θ_k, θ_M). Subscripts *k* and *M* mean kHz and MHz of the spectral impedances. The frequency span 2kHz-1MHz enables to make some distinction between inter- and extracellular data since at the high frequency cellular membrane became transparent. The duration of a single measurement cycle is 4 ms/pixel, and accordingly the duration of the frame scan is ~ 8s for the full frame (64 × 32) or ~ 4s for its half (32 × 32). To register rapid test-induced changes in SEL (the MW and MF stages), the half-matrix scan mode was used. The measurement range: |Z| - from 0.2 to 35 k Ohm, θ – from -90º to +90º. Calibration was carried out at the resistance-capacitance (RC) circuits and showed: mean magnitude relative error 0.2%, mean phase absolute error 0.5º. The spatial non-uniformity of such RC direct transform, caused mainly by the on-resistance scatter of the analogue switches of multiplexer (±20 Ohms, i.e. ~0.1-0.4% of the mean |Z|) was considered insignificant for assessment SEL both: in absolute values and - a fortiori- its relative dynamics. In order to minimize and stabilize the contact impedance, electroconductive gel BEEG Super cream (Cerracarta, Italy) was used. The phantom measurements (pure gelatin 25% w/v in physiological solution) showed the error values in the difference image of two neighboring frames: $\Delta|Z_k|$ = mean ± *б* = -0.01 ± 0.025; $\Delta\theta_k$= mean ± *б* = 0.00 ± 0.008. The noise, originated from the fluctuations of the skin-electrode interface, has

Figure 1: Photos of the SEI experimental set-up and its sensor head (right) - flat multielectrode matrix of 32 × 64 mm², 32 × 64 =2048 stainless steel electrodes of 0.6 × 0.6 mm² each.

Figure 2: Photo of the microwave generator "Threshold-1" («Порог-1» in Russian)and a stationary magnet.

mainly such a pulsed character, that it can significantly interfere only to the dynamics of 1 or 2 neighboring pixels, but not to the analyzed multipixel structures. In addition, the probability of repetition of the peak values ripples in the same pixel in subsequent frames is small, which is also confirmed by the below dispersion maps for each stage of the experiment (15 frames), from which it follows that the topology of dispersion maxima is not accidental, but reflects initial features of the SEL. So, presenting the SEL images, we deemed it advisable not to cut off the values of the ± 2*6* level, but, when necessary (rarely), to use just a weakened palette colors at the level of about ± 1σ.

Testing means and procedure

The following were sequentially used as test means: microwave generator "Threshold-1" («Порог-1» in Russian), stationary magnet (Figure 2), and hypoxia (in the 2d case):

- The "Threshold-1" (production of "Vidguk", Kiev, approved by the Ministry of Health of the USSR for application in 1989) uses a noise generator of extremely low intensity (<0.1 mW/cm² directly at the output) in the microwave band 54-75 GHz [34-36]. Intensive works on of the biological effects of microwaves began in f. USSR early in the 1980s, when an unusually high effectiveness of their action onto a person *in periods, when their normal functioning is disturbed*, had been established [35]. The "Threshold-1" was used as a basic one in developing method of information-wave therapy. The principal difference of this method from other similar ones is the use not of a part, but of the entire range of microwaves. It is believed that in a broad spectrum of radiation, all (or almost all) vibrations with physiologically significant information superimposed on them are necessary to restore the information homeostasis in the affected organs and systems [35,36]. Specifically, with the aid of "Threshold-1", the microwave-induced wavelike phenomena of the SEL had been firstly registered [28]. Now, in the first experiment, the device was (accidental, not intentionally) used twice: 1st time- at about 1 cm distance from the border of the scan area, i.e. with repeatedly reduced the already extremely low-intensive power flow, and the 2d time - directly to the border.
- The ordinary stationary magnet (37 × 50 × 25 mm) created the nonuniform magnetic field at the scanning zone in the range of 20-30 mT. Two versions of magnetic impact were tested: (i) a relatively slow unipolar increase and decrease of the MF marked as MF↓, and (ii) a reversing MF marked as MF↑↓. In the first case, the south pole of the permanent magnet was slowly brought (within a few seconds) close to the scan zone at a distance of about 1 cm, and slowly removed it in 1 min. In the second case, the north, south of the same magnet was quickly brought to the edge of the scan area, and, after about 30s, it was turned over twice within the next 30 seconds, after which it was quickly removed.
- At the beginning of the final –relaxation- stage, a short breath-hold test during ~50s was also used.

Data processing

To evaluate the SEL dynamics, we used: dispersion analysis; graphical analysis of the time curves of selected pixels; image subtraction method; inter-frame and inter-frame correlation analysis between: (i) consecutive images, (ii) time curves of a chosen pixel and all the rest ones, (iii) time curve of means and the rest time curves. In case of a small sample size, e.g., of 10–12 data frames, the Fisher's exact test was performed, according to which correlation r can be considered statistically significant (p< 0.05) if $r \geq 0.5$. In some cases, in order to exclude drift of the background (mainly due to the increasing soaking of the epidermis by conductive cream), the matrices were normalized (MV=0, σ=1).

Results

The general view of the experiment

The general view of the experiment and a photo of the area of investigation are presented in Figure 3. During the experiment, we did not notice that, besides the MM, there is another weakly visible anomaly in the scan area, i.e. some pigmented area of an unidentified origin, which appeared noticeable in the photograph (indicated by a dotted circle). So, the SEL dynamics of this area may also be of some interest. Figure 4 depicts the most representative sub-areas of the SEL: 1) Contour of MM; 2) Central part (primordial nevus?) of the MM; 3) Zone of maximum transformations (ZMT); 4-6) Areas surrounding the ZMT; 7) Part of the pigmentation zone located in the of 32 × 32 scan area; 8) Intermediate area - presumably the invisible continuation of the 7th.

As a whole, the experiment consisted of 10 stages (145 frames): the preliminary full-frame adaptation stage "0": of 10 frames (~3min), following by 8 main stages of the 32 × 32 mm² frames ("I"-"VIII", #20-120, Figure 5), and a final one-"IX"- of 20 full frames. The main stages, from I to VII, included the following tests:

I. No influence (10 frames, all the rest 7 stages consisted of 15 frames);
II. The microwave exposure of vanishingly low intensity - MW1 in the course of the first 10 frames;
III. No influence, relaxation;
IV. The microwave of extremely low intensity MW2 during 10 first frames;
V. Relaxation;
VI. The constant magnetic field MF↓ during first 10 frames;
VII. The reversing MF↑↓ during first 10 frames;
VIII. Relaxation

Figure 5 illustrates the frame-to-frame test-induced changes of the 4 SEL parameters (θ_k, θ_M,$|Z_k|$,$|Z_M|$) at the 32 × 32 area in the form of correlation graphs calculated for each subsequent frame-image matrix relative to the first one.

The high sensitivity of the SEL to the MW and reversing MF was confirmed even in the analysis of means (Figure 5). Of particular note is the unexpectedly pronounced reaction to the breath holding (IX). It is important to emphasize the clearly visible response sequence of different parameters: $|Z_M| \rightarrow |Z_k| \rightarrow \theta_M$ (the θ_k-response seemingly

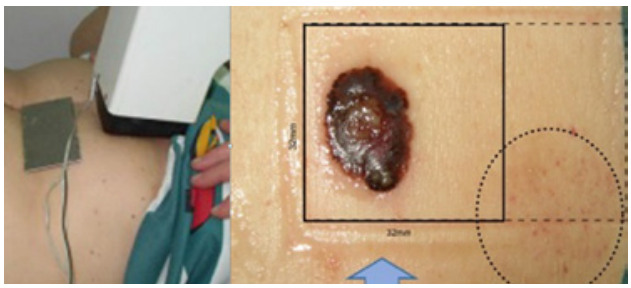

Figure 3: Photos: (i) The scanner placed onto the melanoma area (the ground electrode is placed on the left). (ii) The melanoma area. On the skin, one can see the imprint of the scanner's head. The rectangles denote the 32 × 32 zone of rapid scanning (the solid line) and a full area of investigation (the dotted line). A dashed circle indicates a pigmentation zone of undetermined origin. The blue arrow indicates the direction of the test influences exposures (microwaves and MF).

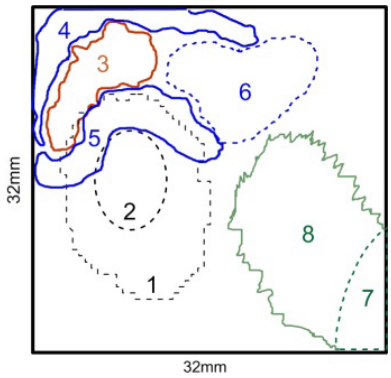

Figure 4: Scheme of the most representative sub-areas of the 32 x 32 zone: 1) Contour of melanoma; 2) Its central part; 3) Zone of maximum transformations (ZMT); 4-6) The areas surrounding the ZMT; 7) A part of the pigmentation zone; 8) An area intermediate between 7 and 6.

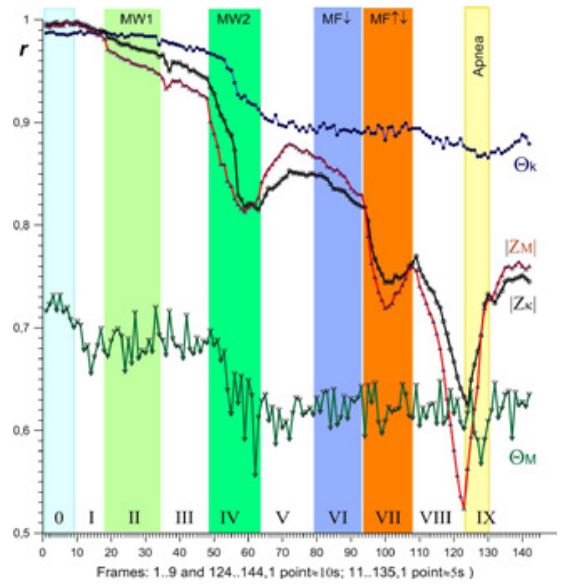

Figure 5: Graphs ofcorrelation between the all current θ_k, θ_M,$|Z_k|$,$|Z_M|$ image matrices and initial one calculated for the 32 × 32 mm^2 area.

have occurred simultaneously with that of $|Z_M|$, although it is not so obvious from the smoother θ_k-graph). Regarding the stages I-VIII, the correlation dependencies can create a false impression that the most significant changes in the SEL are reflected in the parameters of $|Z_k|$ and $|Z_M|$. The subsequent analysis shows that in this case, in order to identify and evaluate clustering process, the change of inter- and intracellular conductivity are less adequate than that of the cooperative dynamics of cell membranes (θ_k, θ_M). This conclusion suggests itself already even when comparing Figure 6 and 7. Thus, our earlier assumption [31], that the topology of such super-high SEL fluctuations was directly related with specificity the MM environment, has been unexpectedly confirmed.

The SEL initial and final dynamics

Figures 6,7 illustrate some stationary and dynamic features of the 0-stage in parameters of θ_k, θ_M, $|Z_k|$,$|Z_M|$, and how their dynamics differ from that of the IX-stage. In particular, from the visual comparative analysis of Figure 6,7 follows:

- Inside central part of MM ("2"), the levels of stationary values of θ_k and θ_M (as well as those of $|Z_k|$ and $|Z_M|$), are almost equal to each other (apart from some difference in absolute values). At the same time, in patterns of θ_k vs θ_M, most external areas of MM (4,5,6,7,8), both in static and dynamic features appear negative to each other.
- There is a noticeable oval spot in the ZMT sector "3" (Figure 6a), the shape and localization of which completely coincides with the epicenter of the subsequent MW-induced transformations. Moreover, it turns out that the dispersion level of the initial fluctuations of θ_k and θ_M (Figure 6 b, e) in relation to the background level has the opposite character. The antiphase character of both -the θ_k vs θ_M and $|Z_k|$ vs $|Z_M|$- fluctuations were also registered between the initial and final stages (Figure 6 c, f and Figure 7c, f respectively). The very phenomenon of existence of such a cluster with the markedly increased intracellular activity compared to the weakened extracellular activity at the tumor boundary seems to us interesting. Here it is worth recalling that, *since there are thousands of cells under each electrode of the matrix, we observe exactly their collective dynamics*.
- The collective antiphase dynamics are also observed between the same parameters in zones "2" and :"7", e.g. Figure 6 b, e and Figure 7.

Figure 8 represents an overview of the test-induced events/changes of θ_k and $|Z_k|$ (in %) happening in each subsequent stage with respect to the preceding one. At the I stage (I-0, Figure 8a, a'), both difference maps θ_k and $|Z_k|$ showed rather chaotic character and do not provide much significant information. The first signs of the MW1-induced clusterization become noticeable in the ZMT ("3") at the II-I map (b,b'). The noticeable clusterization happened as a result of the MW1 after effect during relaxation stage (III-II) can be clearly seen at c,c'. It is worth to emphasize the spatial discrepancy between the θ_k- and $|Z_k|$-structures inside and near the ZMT, and emergence of red coherent structures antiphased to the θ_k-blue at the "4"and "5" sectors. There are also some significant distinctions between the θ_k- and $|Z_k|$-patterns, which enable to contrast the tumor geometry, i.e.: the large blue structure at c) and the red islands at c') around the melanoma perimeter. A noticeable response of the edge of the 7th sector should also be mentioned.

The MW2 stage (d,d') revealed:

- About total decrease of the $|Z_k|$-values including those at the ZMT border; a small (but non-random) increase can only be noted in the center of the melanoma and its periphery;
- Further intensive surrounding ZMT by θ_k (red), and a significant propagation of both structures: the red&blue (i.e. like "crest and hollow") to the left and down - along the outer and inner sides of the melanoma border, presenting, therefore, a single process spreading along the tumor border.

The MF↓ exposure (f,f') seemingly inhibits the source of the wavelike θ_k-activity,i.e.: activity of the "2,3,5" areas. There are two areas of interesting exceptions: in the lower left corner and in "6"; the red structures indicate further propagation of the θ_k-crest. The θk-reaction of the scanned part of zone "7" is also clearly visible.

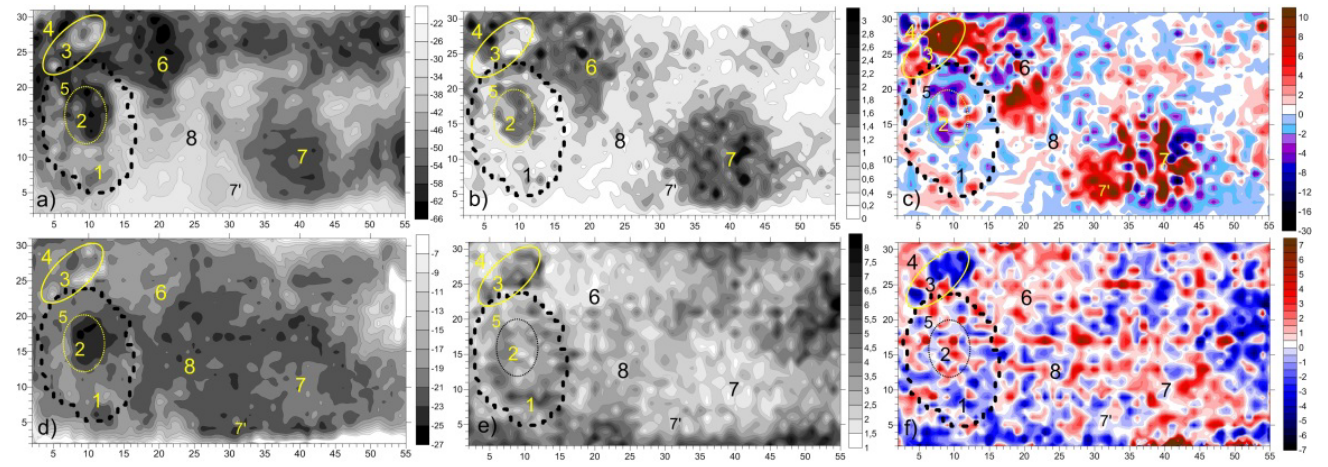

Figure 6: Initial static and dynamic features of θ_k (up) and θ_M (down), and their distinctions from dynamics of the final stages. Correspondingly: a,d) the averaged maps/landscapes (in degrees); b,e) the fields of dispersion (σ); c,f) the 2D distinctions between dispersion maps of stage "0" and that of "IX", ($p<0.01$).

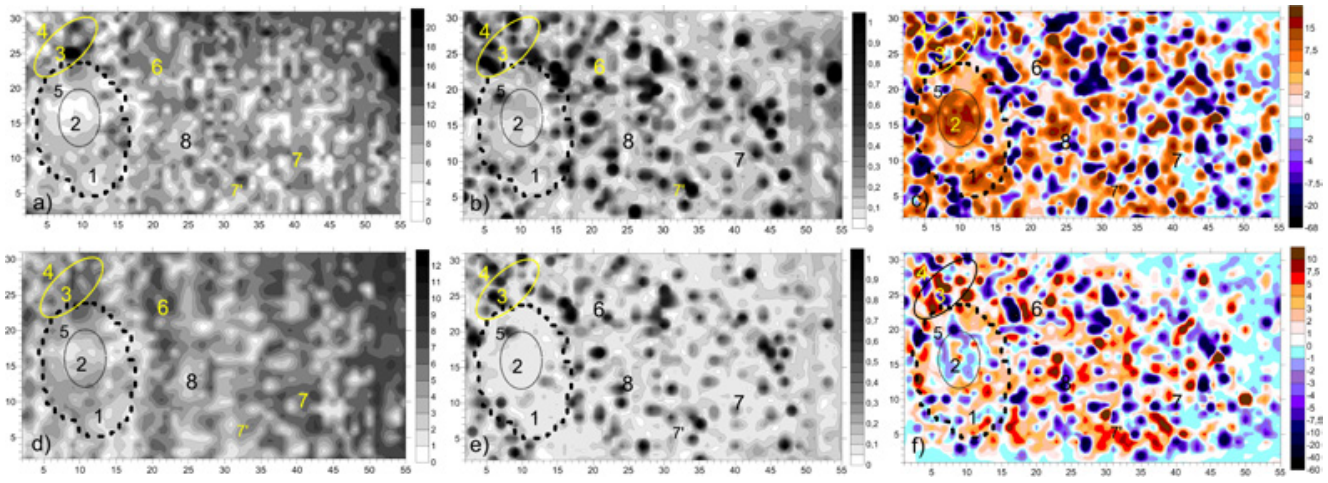

Figure 7: (Similar to Figure 6): a,d)The initial SEL landscapes of $|Z_k|_{AV}$(up) and$|Z_M|_{AV}$(down) (in kOhms); b,e) patterns of their fluctuations (σ); c,f) difference between initial ('0") and final ("IX") patterns of fluctuations, ($p<0.01$).

The $|Z_k|$-response, similarly to d', also has a total character. Against the background of the general rise in the $|Z_k|$-level, a multitude of islands have manifested themselves again in the vicinity of melanoma, especially in the ZMT.

The following exposure of MF↑↓ (g,g') reveals:

- Reverse process of the $|Z_k|$ dynamics (compare g' and e');
- Commonality between the θ_k-process for zone "1" and that of ZMT (increase, red), which has the opposite character with their environment (blue). It may be of interest that the "7" zone has not shown itself clearly enough in all stages.

The final stage of relaxation (h,h') may reflect some mixture of processes that have arisen under the influence of both MW and MF.

The SEL temporal and special dynamics

Figure 9 depicts the temporal dynamics of one of the most active pixels of the ZMT, i.e.: pixel 12 x 26, throughout the whole experiment in parameters of current and average values: $|Z_k|$,$|Z_k|_{AV}$,$|Z_M|$, $|Z_M|_{AV}$, θ_k, $\theta_{k,AV}$, θ_M, $\theta_{M,AV}$.

One can see:

- No pronounced response to the MW1 exposure of all average values;
- Marked transit response to the MW1 exposure of all, but that of $|Z_M|$, current values; the absence of a noticeable response of intracellular conductivity probably indicates the incompleteness of the transmembrane ion exchange, which apparently may explain the transit nature of the whole process. It is assumed that the undulating θ_M-level oscillations, that appeared only during the II-III stages, also evidences in favor of this hypothesis.
- Marked trigger response of all parameters to the MW2 exposure;
- No significant response of all parameters to the MF↓ exposure;
- Noticeable response of all parameters to the MF↑↓ exposure;
- Appearance of significant oscillations of θ_k in response to all impacts, which obviously argues in favor of the well-known hypothesis that cell membranes are the primary target of electromagnetic effects.

Some differences in the diagnostic significance of the special and temporal oscillations of θ_k and $|Z_k|$ can be estimated by analyzing the sequence of corresponding dispersion maps of the I…VIII stages, (Figure 10). Specifically, one can note:

- More structured character of the θ_k-map in all stages, which is particularly evident in displaying the events occurring in the "3-6" zones;
- Noticeably inverse character of θ_k vs $|Z_k|$ in displaying their test-induced dynamics in the "2d" zone and its near surroundings, providing thus some new features of the melanoma geometry;
- Spread of the θ_k-oscillations throughout the scan area during the MF↑↓ exposure (a7), while the $|Z_k|$- changes are hardly noticeable (b7).

In the time domain, in scale interframe changes, corresponding subregions of the θ_k-anomalies were also detected. The correlation fields depicted at Figure 11 show the degree of consistency of the dynamics of each pixel with respect to the average dynamics of all pixels, which allows revealing the cluster character of the SEL dynamics in more details. The clustering effect may have been already emerged even at the preliminary stage I (under the action of the measuring procedure) as a few blue spots exactly in ZMT, and which then multiplied and concentrated there in the II stage. The relaxation stage III (c) reveals a remarkable aftereffect of MW1, i.e. about totally synchronized response with positive correlations throughout the whole scan-area (***r***=0.05...1). Moreover, topology of the areas with minimum ***r*** well coincides with the areas of maximum θ_k-oscillations (Figure 10, a1-a3). The MW2-exposure (d) triggers fast development (within two frames, Figure 9) of distinctly antiphase structures (***r*** ≈±1), i.e. "3" vs "4","5" (Figure 4 e). The MW2-aftereffect, unlike that of MW1, does not cause total synchronization, but only leads to the development of two new antiphase structures (on the border of melanoma), which apparently continue the process that arose in previous stage (Figure 11d**,** bottom left). The MF↓-exposure (Figure 11f) did not cause any noticeable changes. In contrast, the impact of MF↑↓ (Figure 11g) resulted in increased synchronization (***r***=0.4..1), i.e. higher than that of MW2 (c). Worth noting, that this time, the "3" zone was not involved in the synchronization process. The relaxation stage VIII (Figure 11h) looks more informative that the previous one: the state of high synchronization is preserved only in the inactive zones, while the closer to zero correlation ***r*** in the active ones reveals the melanoma core and other features of the scan-area (i.e.: "2,3,4,5,7", Figure 4).

In Figure 12, a few examples of the in-phase and anti-phase dynamics of some pixels located on both sides of the ZMT border are presented. Two such cases (bold curves) indicate a distinct anti-phase response of θ_k to MW2: the pixels 8 × 28 and 6 ×26, located on both sides of the border of ZMT zone (3, Figure 4). Besides, the p8 × 28 demonstrates a particularly marked behavior, i.e. a sound, but somewhat returnable, drop of $|Z_k|$ in response to MW1, near-stable regime during the relaxation (III), a trigger-like response to both MW2, and following resistant equanimity at this lower level during the subsequent stages V-VII. As for the $|Z_k|$ dynamics, there are two interesting pixels bordering on ZMT: (i) p6 × 23 demonstrating marked transient reaction to MW2 followed by a return to its average dynamics; and (ii) p13 × 26, which is out of phase with p6 × 26 in response to both: MW1 and MW2, and also is out of phase with the averaged response to MF↓.

Figures 13 and 14 indicate the existence of zones of coherence/anticoherence with respect to the MW1-induced θ_k- and $|Z_k|$-dynamics of some ZMT pixels. Left: temporal θ_k-curves (running average) of the adjacent pixels (p6 × 24, p6 × 25 and p6 × 26), and the corresponding correlation fields calculated for the joint period of stages II-III (compare with Figure 8c,d,c',d').

The post-MW1 effects can be better can be better understood by correlations over a period of two stages: II and III, since the onset of the θ_k-synchronization in stage III provides a rather blurred mapping (Figure 11c). By calculating such map for the joined period, i.e. including thus differences in the transitional reaction between the II and III stages, we've got a more complete picture of the MW1-effect. This approach, in particular, provides some more detailed information on the boundary differences between in-phase and anti-phase structures. Indeed, the correlation maps (Figure 13a',b') corresponding to the two neighboring p6 × 25 and p6 ×26, located on both sides of the border between the 3rd and 5th zones, are significantly different:

- Their marked anti-phase θ_k-dynamics during the II stage (Figure 13a,b) changes to the in-phase mode already in the last frames of the II stage, i.e. immediately after turning off the MW1;
- The anti-phase structure (zones: 4-6) of Figure 13a (r_{max}=-0.9) strikingly match the θ_k-pattern of the *future response* to MW2 in the next stage;

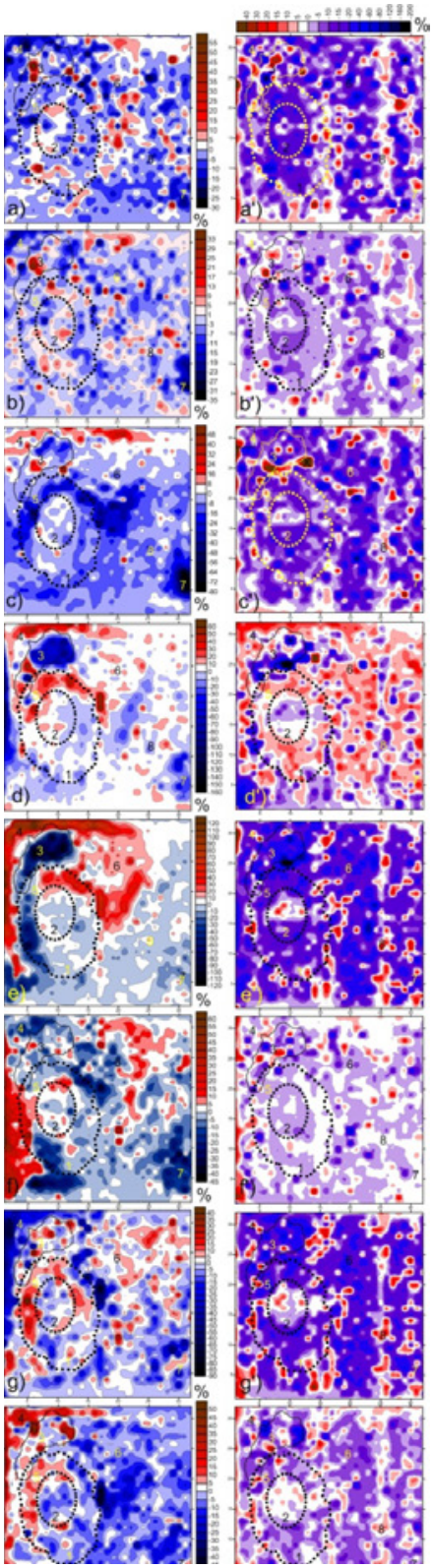

Figure 8: The test-induced SEL transformations calculated as differences of inter-stage averaged image matrices of θ_k (a...g, left column) and $|Z_k|$(a'...g', right column), in %. Top down: I-0, II-I, III-II, IV-III, V-IV, VI-V, VII-VI, VIII-VII.

Notes: 1) Due to significant changes of θ_k, its color range (palette) was chosen not the same but correspond to real values. Otherwise, it would be impossible to consider the topology of the θ_k clustering, in particular its chaotic character in the I-0, II-I images. 2) Red clusters at c' - p5 x 23, p7 x 25, p13 x 25 – are the components of the area of $|Z_k|$-response.

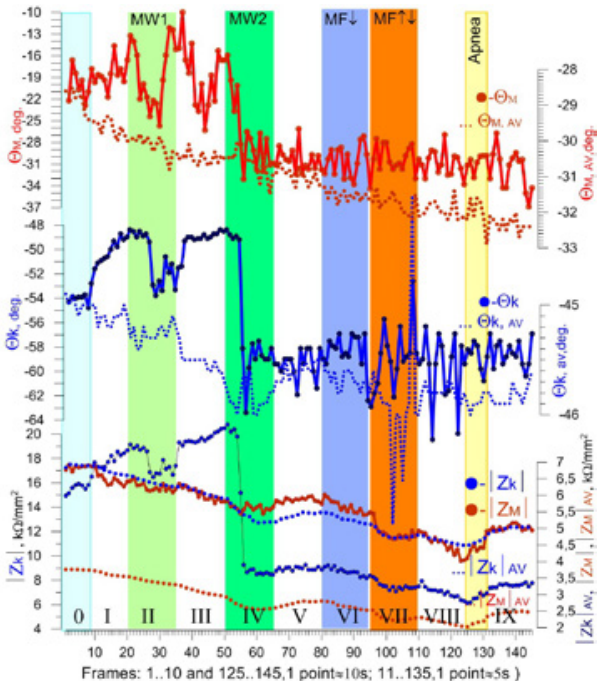

Figure 9: The temporal dynamics of pixel 12 × 26 (one of the most active pixels of the ZMT) during all stages 0...IX, parameters: $|Z_k|$,$|Z_k|_{AV}$.,$|Z_M|$, $|Z_M|_{AV}$, θ_k, $\theta_{k,AV}$, θ_M, $\theta_{M,AV}$

- the red in-phase θ_k-structure on the left coincides with that of the even more distant event - the MW2- aftereffect (Figure 11e);
- The blue structure in the "1" zone (Figure 13b') fully coincides with the lower half of the blue structure of Figure 13b, while its upper half and the "4th" zone are antiphased to the same area of Figure 13b. At the same time, there is also a clearly noticeable difference between Figure 13b and Figure 13b' in the "7th" zone;
- No noticeable differences in the correlation fields of $|Z_k|$ (Figure 13d,d' were found. The probable cause is the spatial mismatch of the active zone $|Z_k|$ (the red structure is below and partly inside the 3d zone) and that of θ_k; as a result, both pixels are inside the $|Z_k|$ -active zone and therefore have the in-phase dynamics.

Figure 15 represents process of the MW2-induced modification of the ZMT and its surroundings, i.e. emergence of the θ_k- and $|Z_k|$-clusters and their interaction in detail.

Of the whole range of the ZMT- metamorphoses, shown at Figure 15, the following events can be noted. At (a,b) and (a',b'), inside zone "3", the two blue sub-clusters - 3' and 3"are seen as separately growing and merging structures. On the way to their merger, there is another developing, but antiphased sub-cluster (pixel p.5 x 23). On (b), the 3 'and 3" merged, encircling (but not devouring) at the same time the p.5 x 23. The one-time emergence of the main- $\Delta\theta_k$ structure (3, red) at (c) give rise to several noticeable processes:

- Remarkably slower red-blue absorption at (c): 3' and 3" disappeared within 30s;
- One-time red-blue absorption of 3' and 3"at (c');
- Abrupt blue-red absorption at the "4" area (keep in mind presence of the blue islands at a,b);
- Propagation of the "4" and "5" structures with a velocity up to 1 cm/min.

It should be recalled here that all these sub-clusters - p5 × 23, p7 × 25 (as well as p13 × 25) - are components of the time averaged $|Z_k|$-structure, i.e. the $|Z_k|$-response to MW2, which clearly manifested itself (as a marked red whole) adjacent and partially penetrating into the "3" zone, Figure 8c').

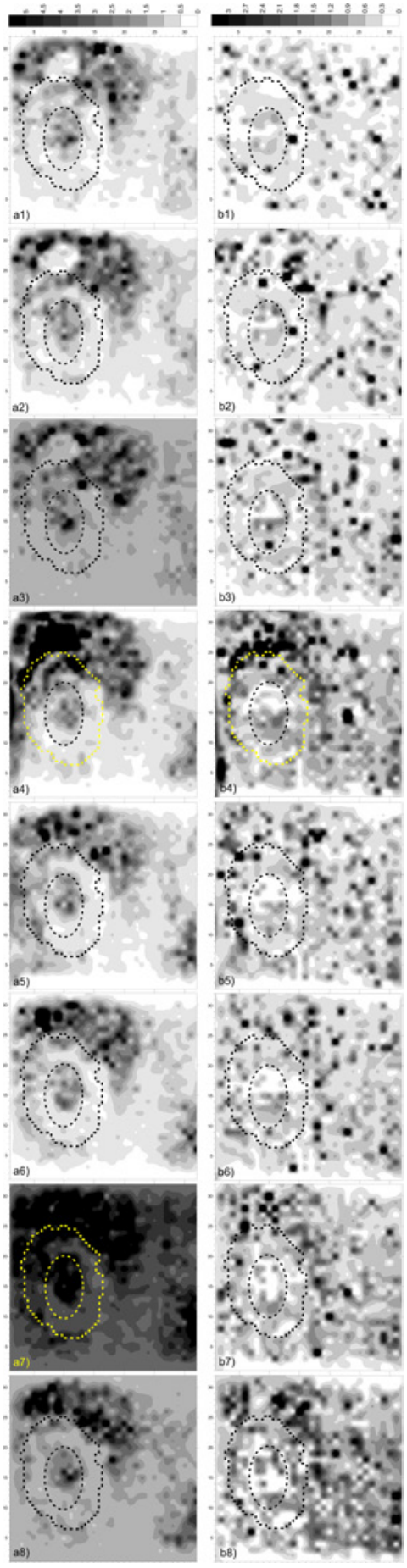

Figure 10: Dispersion fields of θ_k (a1-a8) and $|Z_k|$ (b1-b8) for alll-VIII tages.

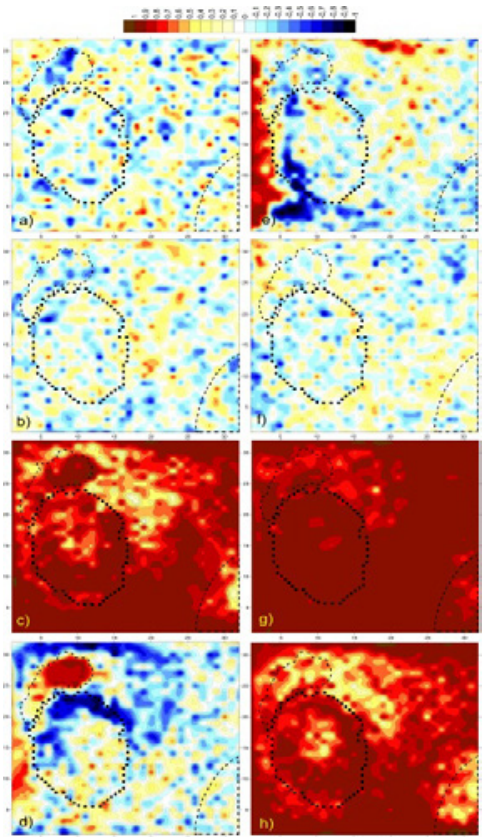

Figure 11: Maps of correlation between frame averaged temporal dynamics ($\theta_{k,AV}$ at Figure 9) and those of the rest pixels throughout the I -VIII stages (a...h, respectfully).

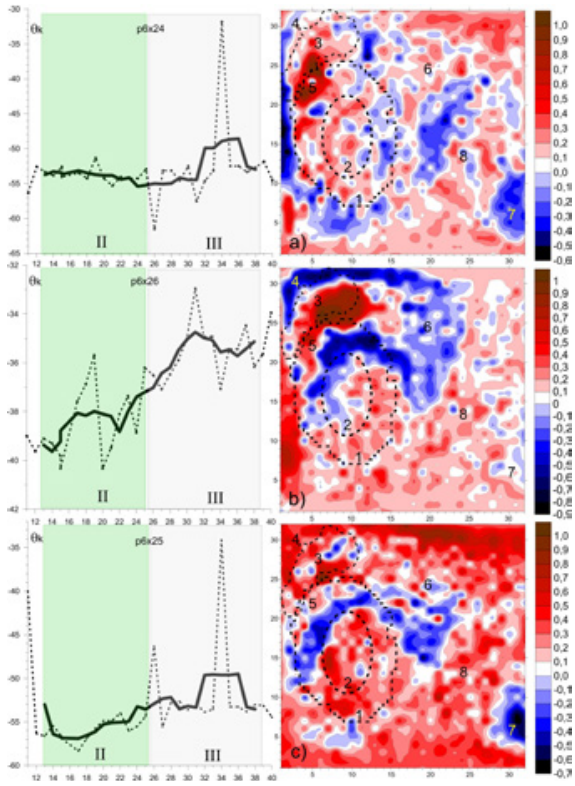

Figure 13: Aftereffects of MW1: the test-induced zones of coherence/anticoherence with respect to the θ_k-dynamics of some ZMT pixels. Left: temporal θ_k -graphs (running average) of the adjacent pixels (p6 × 24, p6 × 25 and p6 × 26), and corresponding correlation fields calculated for joint period of stages II-III.

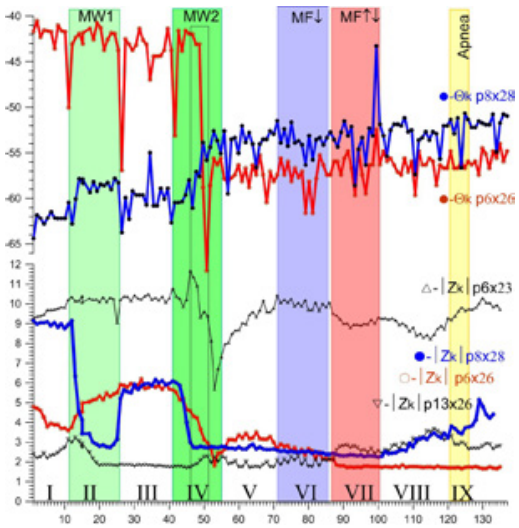

Figure 12: A few examples of the in-phase and anti-phase dynamics of some pixels located on both sides of the ZMT border. Two cases in bold indicate a distinct anti-phase response of θ_k to MW2: the pixels p8 × 28 and p6 × 26, located on both sides of the border of ZMT zone (3, Figure 4).

Discussion

To date, there are numerous experimental and theoretical data about various biological effects of non-thermal MW and MF on cells, cell cultures and tissues [37-43]. However, the question of the mechanisms of these effects and the threshold limits of exposure is still debatable. We assume that our results match to both definitions: (i) that of K. Foster that the threshold field strength is the level below

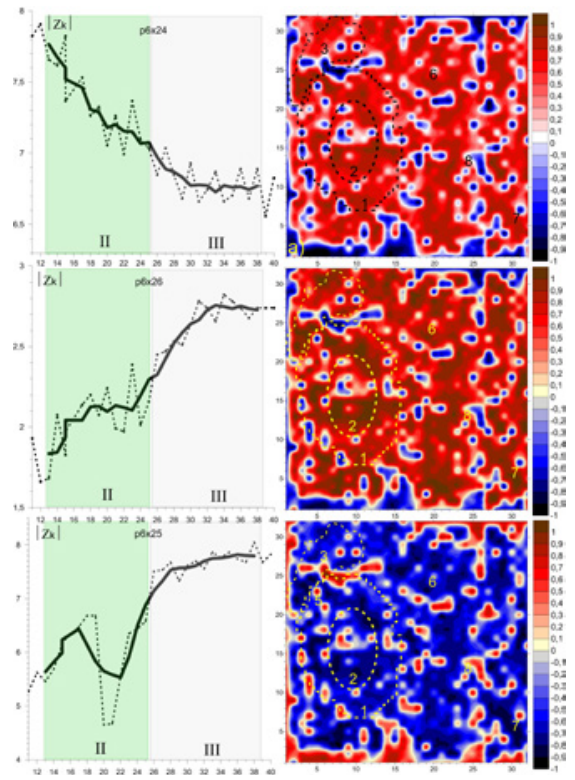

Figure 14: (similar to Figure 13. Aftereffects of MW1: the test-induced zones of coherence/ anticoherence with respect to the $|Z_k|$ -dynamics of some ZMT pixels. Left: temporal $|Z_k|$ -graphs (running average) of the adjacent pixels (p6 × 24, p6 × 25 and p6 × 26), and corresponding correlation fields calculated for joint period of stages II-III.

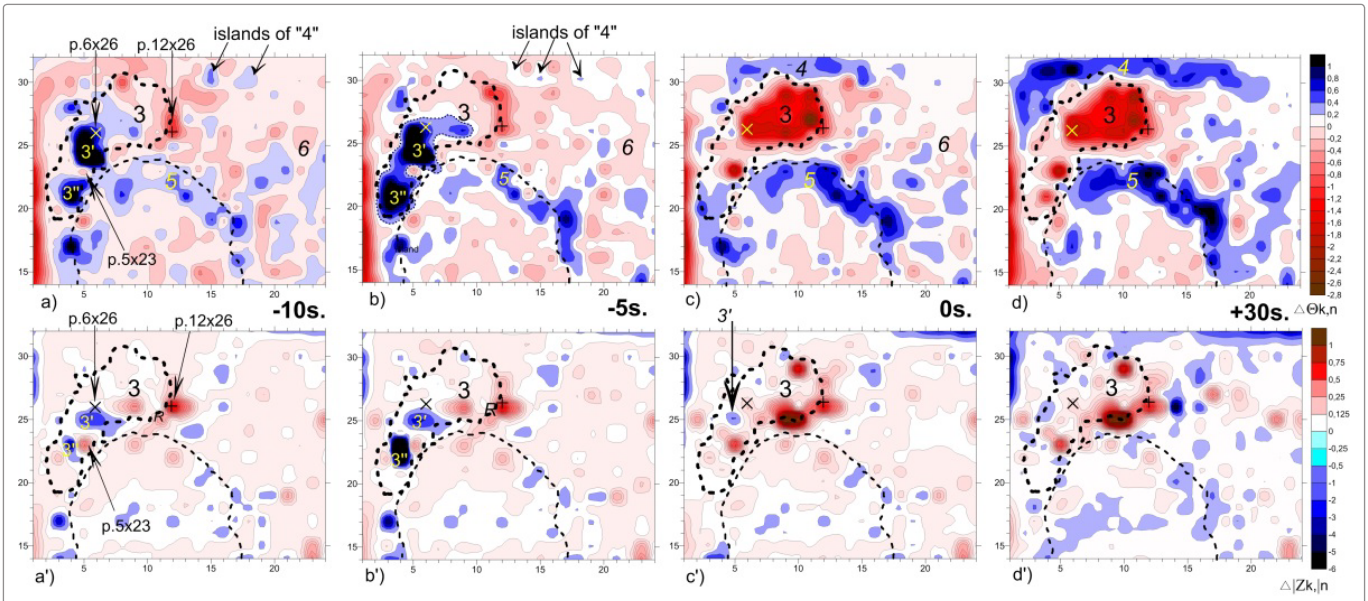

Figure 15: The ZMT dynamics in response to MW2 in normalized difference images of $\Delta\theta_k$ (above) and those of $\Delta|Z_k|$ (below): emergence of the θ_k and $|Z_k|$ clusters and their interaction. Where symbol "Δ" means difference between current image-matrix and that of the 1st frame of the IV stage (#41). Thus, the two left images of each row (a,b; a',b') correspond to the differences (#47-#41) and (#48-#41), i.e. just before (10s and 5s in time domain respectively) the trigger effect emerged at the 49d frame (i.e. #49-#41), which is depicted at the c,c'). The d,d' images correspond to the frame #56 (#56-#41), 30s later. The areas of red and blue correspond to increase and decrease in the values, identifying thus the in-phase and anti-phase clustering.

which no observable response is observed [44] and (ii) that of I. Belyaev [45] that it is what is just above the background level. It should be emphasized here that our case refers to a pathologically altered state of living tissue in which electromagnetic hypersensitivity was caused by oncogenesis. At the same levels of exposure, both to MW and MF, we never observed a noticeable response in healthy tissues. Of note, the applied level of MF, in contrast to that of MW, was within the generally accepted "therapeutic" values, so it is not "slightly above the background", but far exceeds the estimated limit of sensitivity to MF (~10×10^{-6} T [46] *without causing noticeable effects in normal skin*.

Earlier experimental and clinical studies have shown that in the case of the action of non-thermal MW on cells, resonance phenomena are observed; depending on the physiological state of the cell, a variety of effects may occur, including those counter-directed ones, in particular, changes of: sensitivity of membrane transport processes, cooperativity and binding characteristics of the potassium channel activation by internal calcium; structural changes in water surrounding the membranes; lipid peroxidation - antioxidant protection; permeability of blood capillaries; homeostasis and rheological blood properties [35,47-50]. According to [51], MW interacts with tissular water, causing critical hydration of membrane proteins, which ensures their passage from the passive into the active functional state. A healthy/balanced physiological state is characterized by the lowest sensitivity to MW [47].

Although behavior of individual cells is well described, the same cannot be said for cells as part of a "collective". Cells comprising both endothelial and epithelial monolayers clearly exhibit collective effects, such as e.g.: migration of large multi-cellular assemblies: unanticipated fluctuations of mechanical stress that are severe, emerge spontaneously, and ripple across the monolayer. This is clearly a property of collective system and not of any individual cell on its own [49,52]. The MW-induced calcium efflux from the cultured cells had been repeatedly confirmed [53,54]. In principle, calcium waves can mediate the transmission of information from a local site to a global area; the communication of Ca2+ signals to multiple surrounding cells provides the potential to coordinate and synchronize the function of a large group of cells [55,56]. The absence or reduced number of gap junctions and gap-junction intercellular communication, which have been observed in a large number of human and animal tumor cell lines, and whichcan certainly emerge on the SEL pattern [57]. A large number of cellular studies have indicated that MMW may alter structural and functional properties of membranes. The effects of MW radiation on the ion transport may be the consequence of a direct effect on membrane proteins as well as on structural modifications in biomembranes [37,46,58-61]. Oscillations in the concentration of free cytosolic calcium ([Ca2+]) are a ubiquitous signaling mechanism, occurring in many cell types and controlling a wide array of cellular functions. Current understanding of Ca2+ oscillations is based on the concept of the Ca2+ "toolbox". According to this concept, cells can express a range of toolbox components [such as Ca2+ ATPase pumps, voltage-gated Ca2+ channels, or Ca2+ channels in the endoplasmic/sarcoplasmic reticulum (ER/SR) membrane; by changing the spatial and temporal expression of these toolbox components, cells can control exactly where and when [Ca2+] is increased or decreased [62,63]. The complex spatio-temporal calcium dynamics was registered in an epithelial sheet consisting of several 10,000 cells [64].

A number of separate mechanisms regulating intra-and intercellular interrelations have antagonistic effects that balance each other. This circumstance allows the living system to maintain relative dynamic constancy, despite changes in the environment. According to this idea, the effect of MW on healthy people was considered practically insignificant. Since the radiation of the broadband generator "Porog" (used in our experiments) includes all the necessary frequencies (carriers), and the remaining frequencies are harmless, the clinical use of such a generator was considered reasonable and even more preferable [36,47].

All systems in an organism from the molecular to the organ level are more or less in motion. Thus, in living tissue MF affects both excitable and non-excitable cells [65]. The highest (quantum) sensitivity limit to MF was assessed in the range around 10nT [66,67]. There are several mechanisms based on physics of nonequilibrium and nonlinear systems [46] by which MF can affect biological systems: (i) by applying forces to ions or molecules that have magnetic dipole moments; (ii) by modifying the energy levels and the angular momentum of the ions or molecules in the system; (iii) (for time varying MF) via the induced electric field and the corresponding changes in the local electrical currents, changes in spin states and radical concentration [68]. It was also suggested that the cellular response, caused by MF of extremely low frequency, is

similar to that observed with MW radiation [69]. Our results seem to support this hypothesis, as noted above, Figure 11c,f are very similar. As was recently reported, weak MFs affect the production of reactive oxygen species, which in turn alter the cell behavior [70].

Known data on the production of ROS indicate the possibility of its bidirectional response to the MF [71]. For us, it is also tempting to use the ROS factor to explain (i) the unexpected sharp rise/recovery in the correlation curves, and (ii) the large temporal shift between $|Z_M|$ and $|Z_k|$, Figure 5, IX. The hypoxia-induced ROS may be a normal physiological response to an imbalance in oxygen supply, but its role in the mechanisms of a normal response to this stimulus is still uncertain [72]. Also, mitochondria are considered the major source of ROS and under hypoxia, ROS production gets enhanced in several cell lines/animals [73]. Thirdly, as reported in [74], the intracellular calcium oscillations were not influenced by extracellular calcium influx. Such independence might also shed light on the shifts between the curves of the III stage, Figure 5, as well as the noticeable differences between the patterns of $|Z_k|$ and and Θ_k [Figure 13-15].

The phenomena of synchronization and clustering registered in our studies are not exceptional, they are among the fundamental ones in nature. Many biological and physical systems show a tendency to synchronized oscillations in a process termed "dynamical quorum sensing". A broad class of natural and man-made system exhibits rich patterns of cluster synchronization in healthy and diseased states, where different groups of interconnected oscillators converge to cohesive yet distinct behaviors [75]. Many self-oscillatory systems have closely spaced frequencies, and if they are interconnected (e.g., by diffusion), the establishment of synchronous modes is a consequence of the very nature of self-oscillatory systems. In an ensemble of nonideptic oscillators, those whose eigen frequencies are close are able, according to the Kuramoto model [76], to synchronize, and, therefore, synchronization can cover the entire population, or at least most of it. As a result, the regime of chaotic, with the exception of elements that, like malignant cells, behave in a very individualistic manner, becomes rhythmic. In accordance with the pioneering hypothesis of Fröhlich [60], the functionality in living systems results from coherent vibratory states influencing the apparently chaotic motions and arrangements of biological molecules. It is fundamentally important that these coherent states can manifest at large distances, which suggests a mechanism by which cells can interact between and within cells, in addition to the known chemical forces of short-range action. This long-range biological coherence provides the growth control as it exists in healthy tissue, but is absent in cancer. Wherein, cell membranes are considered the main target, sensitive to coherent excitations above 10^9 Hz. A number of researchers have expanded the concept of Fröhlich and are aimed at experimental testing of the predicted conditions [77-86].

The synchronization effects may also be associated with vascular reactions [33,87-90]. Of particular interest is the bidirectional effect [91], i.e. the simultaneous effects of vasodilation and vasoconstriction in response to a much less intense MF (about 1 mT) than ours.

And, finally, taking into account the common origin of the skin and brain (from the same type of the ectoderm), in our opinion, it would be interesting to compare the phenomena of spontaneous and cluster dynamics of the brain with that of the skin, i.e.:"our brain on the outside"[92]. As we have seen: (i) the topology of initial fluctuations SEL corresponds to visible, and then MW/MF-identified skin anomalies [Figure 6,7]; (ii) the MW/MF effects led to emergence of the spatially synchronous or anti-synchronous clusters [Figures 8,11,13-15]. On the other hand, similar phenomena of: (i) "spontaneous low frequency (<0.1 Hz) fluctuations of brain **a**ctivity as measured by resting-state fMRI (on localizing areas of critical function for presurgical planning) have shown to be organized in terms of large-scale functional networks"[93,94]**;** and (ii) in response to weak MFs, the electrical activity of different parts of the brain manifests simultaneously [95] and thus firing patterns of synchronous or anti-synchronous oscillations [96]; and summarizing, the synchronization bridges the structure and the function of various systems, including neural systems [97-100]. There is another interesting analogy between the phenomenon of skin hypersensitivity to EMF (as we have registered in the area altered by the tumorigenesis), and the phenomenon of "electrohypersensitivity" recorded in the brain regions affected by neurotoxins [101-103]. In both cases, these areas can be considered functionally abnormal/empoisoned or homeostatically imbalanced zones.

Conclusions

In this paper, for the first time, on the example of MM and its affected surroundings, we present experimental evidence and alleged theoretical background of novel phenomena in living matter:clusterization and synchronization of electrodynamic landscape. These phenomena:

- unlike those of conventional electrophysiology, belong to the tissues of non-excitable cells;
- manifest themselves in the functionally abnormal areas in a form of initial or test-induced clusters of coherent and anticoherent oscillations. The clusters can interact and move;
- may forecast SEL events on cellular level by detecting prior changes at the intracellular level;
- are assumed to be macroscopic/tissue manifestations of homeostatic imbalance at inter- and intracellular, and probably molecular levels;
- are presumably associated with cooperative mechanisms of short- and long-range intercellular interactions (also taking into account the "quantum bio" version as the most intriguing [104].

The calculated maps of synchronicity corresponded to the visible tumor signs and significantly exceeded them in detail and prevalence, thus revealing the hypo/hypersensitive areas of functional heterogeneity. The discovered phenomena may be helpful specifically for real-time mapping the tumor geometry and its affected surroundings, thus providing biofeedback and additional opportunities for cancer research, diagnosis, personalized treatment and surgery, as well as in various biomedical applications.

Acknowledgements

We express our sincere gratitude for the feasible assistance to: Prof. Jacques Jossinet, Mrs. Sharon M. Weinstein, Prof. Michail Y. Antomonov, and Prof. Vitaliy B. Maksymenko. And of course, under our circumstances of the state collapsing, development of this initiative project would hardly have been possible without the USA & Canada grant (#1822, http://www.stcu.int)

Compliance with Ethical Standards

All procedures performed in studies involving human participants were in accordance with the ethical standards of the institutional and/or national research committee and with the 1964 Helsinki declaration and its later amendments or comparable ethical standards.

References

1. Tabassum D, Polyak K. Tumorigenesis: it takes a village. Nature Reviews. Cancer. 2015 Aug;15(8):473-483.
2. Hanahan D, Weinberg RA. Hallmarks of cancer: the next generation. Cell. 2011 Mar;144(5);646-674.
3. Sánchez-Danés A, Hannezo E, Larsimont J, Liagre M, Youssef K, et al. Defining the clonal dynamics leading to mouse skin tumor initiation. Nature. 2016 Aug;18;536(7616):298-303.
4. Chapman A, Fernandez L, Ferguson J, Kamarashev J, Hurlstone A. Heterogeneous tumor sub populations cooperate to drive invasion. Cell Rep. 2014 Jul;8:688-695.
5. Wang J, Egnot B, Paluh J. Cell Competition and Cooperation in Tissue Development. J Tissue Sci Eng 2016 Jan;7:131.
6. Bertolaso M, Dieli A. Cancer and intercellular cooperation. R Soc Open Sci. 2017 Oct;4(10):170470.

7. Martincorena I, Roshan A, Gerstung M, Ellis P, Loo P, et al. Tumor Evolution. High burden and pervasive positive selection of somatic mutations in normal human skin. Science. 2015 May;348(6237):880-886.
8. Cova C, Abril M, Bellosta P, Gallant P, Johnston, et al. Drosophila myc regulates organ size by inducing cell competition. Cell. 2004 Apr;117(1)107-116.
9. Lynch M, Lynch C, Craythorne E, Liakath-Ali K, Mallipeddi R, et al. Spatial constraints govern competition of mutant clones in human epidermis. Nature Communications. 2017 Oct;8:1119.
10. Natrajan R, Sailem H, Mardakheh F, Garcia M, Tape C, et al. Microenvironmental Heterogeneity Parallels Breast Cancer Progression: A Histology-Genomic Integration Analysis. PLoS Med. 2016 Feb;13(2)132: e1001961.
11. Funk R. Endogenous electric fields as guiding cue for cell migration. Front Physiol. 2015 May;6:143.
12. Salari V, Barzanjeh Sh, Cifra M, Simon C, Scholkmann F, et al. Towards non-invasive cancer diagnostics and treatment based on electromagnetic fields, optomechanics and microtubules. arXiv. 2017 Aug;1708.08339v1.
13. Fink C, Haenssle, H. Invited Review: Non-invasive tools for the diagnosis of cutaneous melanoma. Skin Res Technol. 2017 Aug;23(3):261-271.
14. Canali C, Mazzoni C, Larsen LB, Heiskanen A, Martinsen, Ø G, et al. An impedance method for spatial sensing of 3D cell constructs--towards applications in tissue engineering. Analyst. 2015 Sep;140(17):6079-6088.
15. Canali C, Heiskanen A, Muhammad HB, Høyum, P, Pettersen, FJ, et al. Bioimpedance monitoring of 3D cell culturing--Complementary electrode configurations for enhanced spatial sensitivity. Biosens Bioelectron. 2015 Jan;63:72-79.
16. Martinsen, ØG, Grimnes, S. Bioimpedance and bioelectricity basics. 3rd ed.. London, UK: Academic Press. 2014.
17. Gheorghiu E, Asami K. Monitoring cell cycle by impedance spectroscopy: experimental and theoretical aspects. Bioelectrochem Bioenerg. 1998 May;45(2):139-143.
18. Rocha L, Menzies S, Lo S, Avramidis M, Khoury R, Jackett L. et al. Analysis of an electrical impedance spectroscopy system in short-term digital dermoscopy imaging of melanocytic lesions. Br J Dermatol. 2017 Nov;177(5):1432-1438.
19. Mohr. P, Birgersson U, Berking C, Henderson C, Trefzer U, et al. Electrical impedance spectroscopy as a potential adjunct diagnostic tool for cutaneous melanoma. Skin Res Technol. 2013 May;19(2):75-83.
20. Ceder H, SjöholmHylén A. WennbergLarkö AM, Paoli J. Evaluation of electrical impedance spectroscopy as an adjunct to dermoscopy in short-term monitoring of atypical melanocytic lesions. Dermatol Pract Concept. 2016 Oct;6(4):1-6.
21. Aberg P, Birgersson U, Elsner P Mohr P, Ollmar S. Electrical impedance spectroscopy and the diagnostic accuracy for malignant melanoma. Exp Dermatol. 2011 Aug;20(8):648-652.
22. Ollmar S, Grant S. Nevisense: improving the accuracy of diagnosing melanoma. Melanoma Manag. 2016 Jun;3(2):93-96.
23. Nicander I, Emtestam L, Åberg P, Ollmar S. Twelve years evolution of skin as seen by electrical impedance. J Phys Conf Ser. 2010; 224 012092.
24. Braun RP, Mangana J, Goldinger S, French L, Dummer R, et al. Electrical Impedance Spectroscopy in Skin Cancer Diagnosis. Dermatol Clin. 2017 Oct; 35 (4): 489-493.
25. Chiang Y, Jang LS, Tsai SL, Chen MK, Wang MH. Impedance Analysis of Single Melanoma Cells in Microfluidic Devices. Electroanalysis. 2014 Sep;10:2129-2137.
26. Rimi L, Lee SM, Kim HJ, Kim SY, Son M, et al. Dielectric imaging for differentiation between cancer and inflammation in vivo. Scientific Reports. 2017 Oct;7:13137.
27. Babich Y. 1992. Impedanz-Bild Introscopie von biologischen GewebeVer-fahren [Impedance image Introscopy of biological tissue-driving]. Deutsche Zeitschrift fr Akupunktur. 1992;35(4):Ss.93-97.
28. Babich Y. The skin 2D electrobioimpedance response to a remote non-thermal mm-EMF exposure. In: Proc. of 2d Int. Conf. on Bioelectromagnetisml 1998. Melbourne. IEEE 1998.p.79-80.
29. Babich, Y. Quasi stationary and autowave structures of the skin electrobioimpedance relief. 2000. Reports of the Ukrainian NAS.4:199-204.
30. Babich Y. Visualization of the skin spatio-temporal electrical parameters for revealing their characteristic changes in Russian. [dissertation]. Ukraine (UKR): Kiev: Natl Tech University of Ukraine; 2001.
31. Babich YF. Cancer Problem in the Eyes of the Skin Multiparameter Electrophysiological Imaging. In: Burdyuza V, Editor. The Future of Life and the Future of our Civilization. Springer; 2006. p.307-321.
32. Babich Y, Nuzhdina M. Visualization of the Skin Electrodynamic Landscape: Some Phenomenological Features in Norm and Oncopathology., In: Proc. of the World Congress on Medical Physics and Biomedical Engineering. Munich (DE). Springer; 2009. p.1-4.
33. Babich Y, Nuzhdina, M, Syniuta S. Young and advanced tumor-some 2D electrodynamic distinctions: melanoma and satellite during a vascular ocusion test: feasibility study. Med Biol Eng Comput. 2018 Feb;56(2):211-220.
34. Sitko SP, Kolbun ND, inventors; Device for microwave reflexotherapy "Threshold" journal "Electronic industry",l: 1 159, p. 30, author's Certificate SU N1611345 A1 MKI -a 61 N 5/02 1987.
35. Bessonov AE, Millimeter waves in the clinical medicine. A book in Russian, Moscow, 1997;p 240.
36. Kolbun ND, Bessonov AE, Volyanyuk RE. Informational and Wave Therapy. Kiev. Ukr encycl. 1993;304.
37. Markov MS. Electromagnetic Fields in Biology and Medicine. 1st ed. Florida (US). CRC Press. 2017.
38. Belyaev I. Non-thermal Biological Effects of Microwaves. Microwave Review. 2005 Nov;13-29.
39. Tenuzzo B, Chionna A, Panzarini E, Lanubile R, Tarantino P, et al. Biological effects of 6 mT static magnetic fields: a comparative study in different cell types. Bioelectromagnetics. 2006 Oct;27(7):560-77.
40. Shckorbatov Y, Katrich V, Pasiuga V, Rudenko A. Cell Response to Electromagnetic Field: Nuclear and Membrane Mechanisms. New York (USA). Nova Biomedical: 2013. p.133.
41. Bauréus Koch CLM, Sommarin M, Persson BRR, Salford LG, Eberhardt JL, Interaction between weak low frequency magnetic fields and cell membranes. Bioelectromagnetics. 2003 Sep;24(6):395-402.
42. Vecchia P, Matthes R, Ziegelberger, G, Lin, J, Saunders, R, et al. Exposure to high frequency electromagnetic fields, biological effects and health consequences 100 kHz-300 GHz. Review of the scientific evidence on dosimetry, biological effects, epidemiological observations, and health consequences concerning exposure to high frequency electromagnetic fields 100 kHz to 300 GHz. International Commission on Non-Ionizing Radiation Protection. 2009.
43. Williams JM. Biological Thermal and Nonthermal Mechanisms. 2016 Sep;4(7):1-49.
44. Foster K, Thermal and Nonthermal Mechanisms of Interaction of Radio-Frequency Energy with Biological Systems. IEEE Transactions on Plasma Science. 2000 Feb;28(1):15-23.
45. Belyaev IY. Biophysical Mechanisms for Nonthermal Microwave Effects. In: Markov MS. Editor. Electromagnetic Fields in Biology and Medicine. CRC Press. 2017, p. 49-67.

46. Binhi V. Primary physical mechanism of the biological effects of weak magnetic fields. Biophysics. 2016 May;61(1):170-176.
47. Devyatkov ND, Golant MB, Betsky OV. Millimeter waves - M: Technosphere. 2001-2210.
48. Geletyuk V, Kazachenko V, Chemeris N, Fesenko E. Dual effects of microwaves on single Ca2+-activated K+ channels in cultured kidney cells Vero. FEBS Letters. 1995 Feb;359(1):85-88.
49. Andreev V, Betskii O, Ilina S, Kazarinov K, Putvinskii A. In: Nonthermal Effects of Extremely High Frequency Electromagnetic Radiation. Moscow (RU). 1981:167-176.
50. Fesenko E, Gluvstein A. Changes in the state of water, induced by radiofrequency electromagnetic fields. FEBS Lett. 1995 Jun;367(1):53-55.
51. Grenier K, Dubuc D, Chen T, Artis F, Chretiennot T, et al. Recent Advances in Microwave-Based Dielectric Spectroscopy at the Cellular Level for Cancer Investigations. IEEE Transactions on Microwave Theory and Techniques. 2013;61(5): 5.
52. Tambe,D, Hardin,C, Angelini,T, Rajendran,K.Collective cell guidance by cooperative intercellular forces 2011 Nature Materials.10:469-475.
53. Sun S, Liu Y, Lipsky S, Cho M. Physical manipulation of calcium oscillations facilitates osteodifferentiation of human mesenchymal stem cells. FASEB J. 2007 May;21(7):1472-1480.
54. Blackman CF, Benane SG, Joines WT, Hollis MA. House DE. Calcium-ion efflux from brain tissue: power-density versus internal field-intensity dependencies at 50-MHz RF radiation. Bioelectromagnetics. 1980;1(3):277-83.
55. Leybaert L. Sanderson MJ. Intracellular Ca2+ waves: mechanisms and function. Physiological reviews. 2012 Jul;92(3):1359-1392.
56. Pall M. Electromagnetic fields act via activation of voltage-gated calcium channels to produce beneficial or adverse effects. J Cell Mol Med. 2013 Aug;17(8):958-965.
57. Korkiamäki T, Ylä-Outinen H, Koivunen J, Karvonen SL, Peltonen J, et al. Altered Calcium-Mediated Cell Signaling in Keratinocytes Cultured from Patients with Neurofibromatosis Type 1. Am J Pathol. 2002 Jun;160(6):1981-1990.
58. Ramundo-Orlando A. Effects of millimeter waves radiation on cell membrane. Review. J Infrared MilliTerahz Waves. 2010 Dec;31(12):1400-1411.
59. Zhadobov M, Chahat N, Sauleau R, Quement C, Drean Y. Millimeter-wave interactions with the human body: state of knowledge and recent advances International Journal of Microwave and Wireless Technologies. 2011 Mar; 3(2):237-247.
60. Fröhlich H. Long-range coherence and energy storage in biological systems. Int J Quantum Chem. 1968 Sep;2(5):641-649.
61. Goodman R, Blank M. Insights into electromagnetic interaction mechanisms. J Cell Physiol. 2002 Jul;192(1):16-22.
62. Berridge MJ, Lipp P, Bootman MD. The versatility and universality of calcium signalling. Nat Rev Mol Cell Biol. 2000 Oct;1(1):11-21.
63. Sneyd J, Min Han J, Wang L, ChenJ, Yang X, et al. On the dynamical structure of calcium oscillations. Proc Natl Acad Sci U S A. 2017 Feb;114(7):1456-1461.
64. Balaji R, Bielmeier C, Harz H, Bates J, Stadler C, et al. Calcium spikes, waves and oscillations in a large, patterned epithelial tissue. Sci Rep. 2017 Feb;20;7:42786.
65. Leybaert L, Sanderson M J. Intercellular Ca2+ waves: mechanisms and function. Physiological reviews. 2012 Jul;92(3);1359-1392.
66. Wey H, Conover D, Mathias P, Toraason M, Lotz W. 50-Hertz magnetic field and calcium transients in Jurkat cells: results of a research and public information dissemination RAPID program study. 2000 Feb;108(2):135-140.
67. Cai J, Caruso F, Plenio MB. Quantum limits for the magnetic sensitivity of a chemical compass. Phys Rev A. 2012 Apr; 85:040304R.
68. Barnes FS, Greenebaum B. The effects of weak magnetic fields on radical pairs.2015 Bioelectromagnetics. 2015 Jan;36(1):45-54.
69. Kapri-Pardes E, Hanoch T, Maik-Rachline G. Maik-Rachline G, Murbach M. et al. Activation of Signaling Cascades by Weak Extremely Low Frequency Electromagnetic Fields. Cell Physiol Biochem. 2017;43(4):1533-1546.
70. Van Huizen AV, Morton JM, Kinsey LJ, Von Kannon DG, Saad MA, et al. Weak magnetic fields alter stem cell-mediated growth. Sci Adv. 2019 Jan;5(1):eaau7201.
71. Wang H, Zhang X. Magnetic Fields and Reactive Oxygen Species. Int J Mol Sci. 2017 Oct;18(10): 2175.
72. Clanton TL. Hypoxia-induced reactive oxygen species formation in skeletal muscle. J Appl Physiol (1985). 2007 Jun;102(6):2379-2388.
73. Kalogeris T, Bao Y, Korthuis RJ. Mitochondrial reactive oxygen species: A double edged sword in ischemia/reperfusion vs preconditioning. Redox Biol. 2014 Jun;2:702-714.
74. Wang T, Zhou C, Tang A, Wang S, Chai Z. 2006. Cellular mechanism for spontaneous calcium oscillations in astrocytes. Acta Pharmacol Sin. 2006 Jul;27(7):861-888.
75. Favaretto C, Cenedese A, Pasqualetti F. Cluster Synchronization in Networks of Kuramoto Oscillators. IFAC Papers OnLine. 2017 Jul;50(1):2433-2438.
76. Walleczek J. The frontiers and challenges of biodynamics research. Cambridge University Press. 2001.
77. Meijer D, Geesink H. Favourable and Unfavourable EMF Frequency Patterns in Cancer: Perspectives for Improved Therapy and Prevention. Journal of Cancer Therapy. 2018 Mar;9(3):188-230.
78. Nikolov N, Loshitsky P, Solyar A. Synchronization of biological tissues with the medium with complete mixing as the substantiation of a spatially inhomogeneous field under electromagnetic irradiation of tumors. Cybernetics and comput. equipment. 2014:p.63-73.
79. Pokorný J, Vedruccio C, Cifra M, Kučera O. Cancer physics: diagnostics based on damped cellular elastoelectrical vibrations in microtubules. Eur Biophys J. 2011 Jun;40(6):747-759.
80. Lundholm IV, Rodilla H, Wahlgren WY, Duelli A, Bourenkov G, et al. Terahertz Radiation Induces Nonthermal Structural Changes Associated with Frohlich Condensation in a Protein Crystal. Struct Dyn. 2015;2(5):054702.
81. Haken H. Synergetics, an Introduction: Nonequilibrium Phase Transitions and Self-organization in Physics, Chemistry and Biology. New York: Springer-Verlag; 1983.
82. Mäs M, Flache A, Helbing D. 2010. Individualization as driving force of clustering phenomena in humans. PLoS Comput Biol. 2010 Oct 21;6(10):e1000959.
83. MuehsamD, Ventura C. Life Rhythm as a Symphony of Oscillatory Patterns: Electromagnetic Energy and Sound Vibration Modulates Gene Expression for Biological Signaling and Healing. Glob Adv Health Med. 2014 Mar;3(2):40-55.
84. Pilla A, Fitzsimmons R, Muehsam D, Wu J, Rohde C, et al. Electromagnetic fields as first messenger in biological signaling: Application to calmodulin-dependent signaling in tissue repair. Biochim Biochim Biophys Acta. 2011 Dec;1810(12):1236-1245.
85. Jerman I. The Origin of Life from Quantum Vacuum, Water and Polar Molecules.American Journal of Modern Physics. 2016 Jul;5(4-1):34-43.
86. Škarja M, Jerman I, Ružič R, Leskovar RT, Jejčič L. Electric Field Absorption and Emission as an Indicator of Active Electromagnetic Nature of Organisms-Preliminary Report. Electromagn Biol Med. 2009;28(1):85-95.

87. Nagy J, Chang S, Dvorak A, Dvorak H. Why are tumor blood vessels abnormal and why is it important to know? Br J Cancer. 2009 Mar;100(6):865-869.

88. Netti P, Roberge S, Boucher Y, Baxter L, Jain R. Effect of transvascular fluid exchange on pressure-flow relationship in tumors: a proposed mechanism for tumor blood flow heterogeneity. Microvasc Res. 1996 Jul;52(1):27-46.

89. Swartz M, Lund A. Lymphatic and interstitial flow in the tumor microenvironment: linking mechanobiology with immunity. Nature Reviews. Nat Rev Cancer. 2012 Feb;12(3):210-219.

90. Tankanag AV, Grinevich AA, Tikhonova IV, Chaplygina AV, Chemeris NK. Phase Synchronization of Skin Blood Flow Oscillations in Humans under Asymmetric Local Heating. Biophysics. 2017 Jul; 62(4): 629–635.

91. Ohkubo, C, Okano H, Magnetic Field Influences on the Microcirculation In a book: Electromagnetic Fields in Biology and Medicine 1st Ed,CRC Press, ISBN 9781138749030 - CAT# K32708, 2017.

92. Tobin DJ. 2017. Introduction to skin aging.J Tissue Viability. 261:37-46.

93. Biswal B, Yetkin FZ, Haughton VM, Hyde JS. Functional connectivity in the motor cortex of resting human brain using echo-planar MRI.MagnReson Med. 1995 344:537-41.

94. Shimony JS, Zhang D, Johnston JM, Fox MD, Roy A, Leuthardt EC. 2009.Resting-state spontaneous fluctuations in brain activity: a new paradigm for presurgical planning using fMRI. AcadRadiol.

95. Zhadin MN. Review of Russian Literature on Biological Action of DC and Low-Frequency AC Magnetic Fields. Bioelectromagnetics. 2001;22:27-45.

96. Goel P, Ermentrout B. Synchrony, stability, and firing patterns in pulse-coupled oscillators. Physica D. 2002; 163:191-216.

97. Zemanova L, Zhou C, Kurths J. Structural and functional clusters of complex brain networks. Physica D. 224 2006;202-212 .

98. DumasG, LachatF, MartinerieJ, NadelJ, GeorgeN. From social behaviour to brain synchronization: Review and perspectives in hyperscanning. IRBM. 2011;321:48-53.

99. Budzinski R C, Boaretto BRR, Prado TL, Lopes SR. Phase synchronization and intermittent behavior in healthy and Alzheimer-affected human-brain-based neural network Phys. Rev. 2019, E 99, 022402.

100. Erra RG, Jose L,Velazquez P, Rosenblum M. Neural Synchronization from the Perspective of Non-linear Dynamics Front Comput Neurosci. 2017.

101. Heuser G, HeuserSia A. 2017. Functional brain MRI in patients complaining of electrohypersensitivity after long term exposure to electromagnetic fields.Reviews on Environmental Health, Rev Environ Health. 26;323:291-299.

102. Chen Y, Lyga J. Brain-skin connection: stress, inflammation and skin aging. . Inflamm Allergy Drug Targets. 2014;133:177-90. Slominski AT, Zmijewski MA, Skobowiat C, Zbytek B, Slominski

103. RM, et al. Sensing the environment: regulation of local and global homeostasis by the skin's neuroendocrine system. AdvAnatEmbryol Cell Biol. 2012;212:v, vii, 1-115.

104. Offord C. Quantum Biology May Help Solve Some of Life's Greatest Mysteries. The Scientist. 1 June 2019